Sau et al., http://www.jcb.org/cgi/content/full/jcb.201312002/DC1

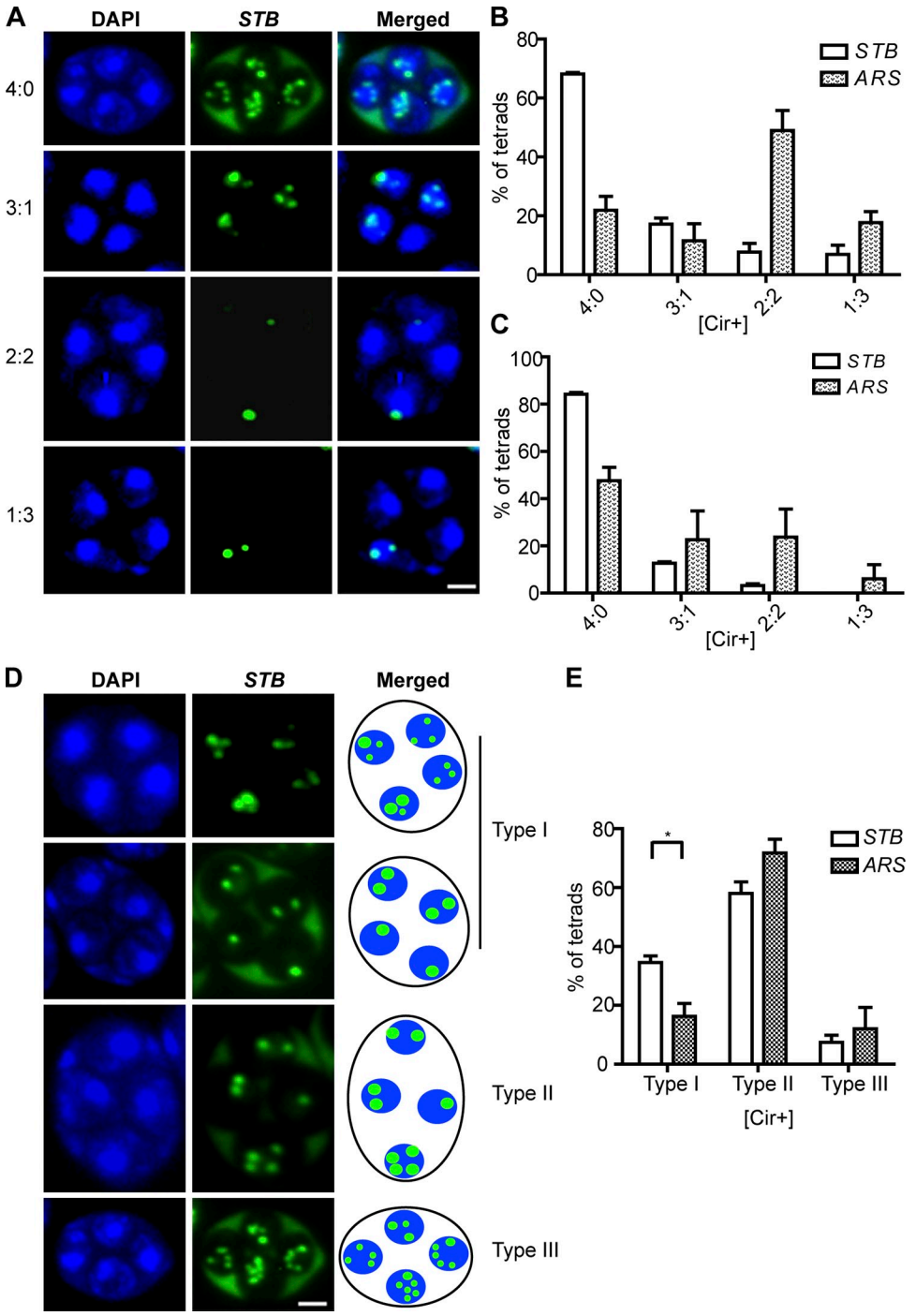

Figure S1. ***STB* and *ARS* plasmid distribution in spores: classification of tetrads containing plasmid foci in all four spores.** (A and B) The assays were performed in a [cir+] strain. Individual tetrads were classified in terms of the number of plasmid-bearing spores that they harbored: 4:0, 3:1, 2:2, and 1:3, with the first number in these ratios indicating plasmid-containing spores. The mean plasmid foci counts per tetrad for the *STB* plasmid were 8.8, 4.5, 3.4, and 1.4 for the 4:0, 3:1, 2:2, and 1:3 classes, respectively. The corresponding values for the *ARS* plasmid were 9.8, 6.6, 2.8, and 2.0. (C) In this histogram representation, tetrads containing a total of fewer than four plasmid foci were excluded from the analysis. The meiosis II assays represented by this figure were performed separately from the meiosis I assays depicted in Fig. 1. The fact that only ~1% of the binucleate cells were devoid of the *STB* plasmid (Fig. 1 C), whereas ~15% of the asci lacked plasmid foci in two or more spores (2:2 and 1:3 classes in B) suggests that plasmid loss in spores is primarily caused by missegregation events during the second meiotic division. There is a caveat that these classes of asci contain fewer plasmid foci than the 4:0 and 3:1 classes. Note the reduction in the 2:2 and 1:3 classes when only those tetrads with at least four foci were included in the analysis (C). (D) The tetrads shown represent the three types (I–III) into which the 4:0 class was subdivided, based on the number of plasmid foci in individual spores. Type I included two classes: asci in which all four spores or two pairs of spores, but not all four spores, contained equal number of foci. Type II asci contained only one pair of equal-foci spores, whereas type III asci were unequal in all four spores. (E) The relative proportions of the three types of tetrads observed for the *STB* and *ARS* reporter plasmids were plotted. The error bars indicate ± SEM (standard error of the mean). *, $P < 0.05$ (two-tailed *t* test). Bars, 2 µm.

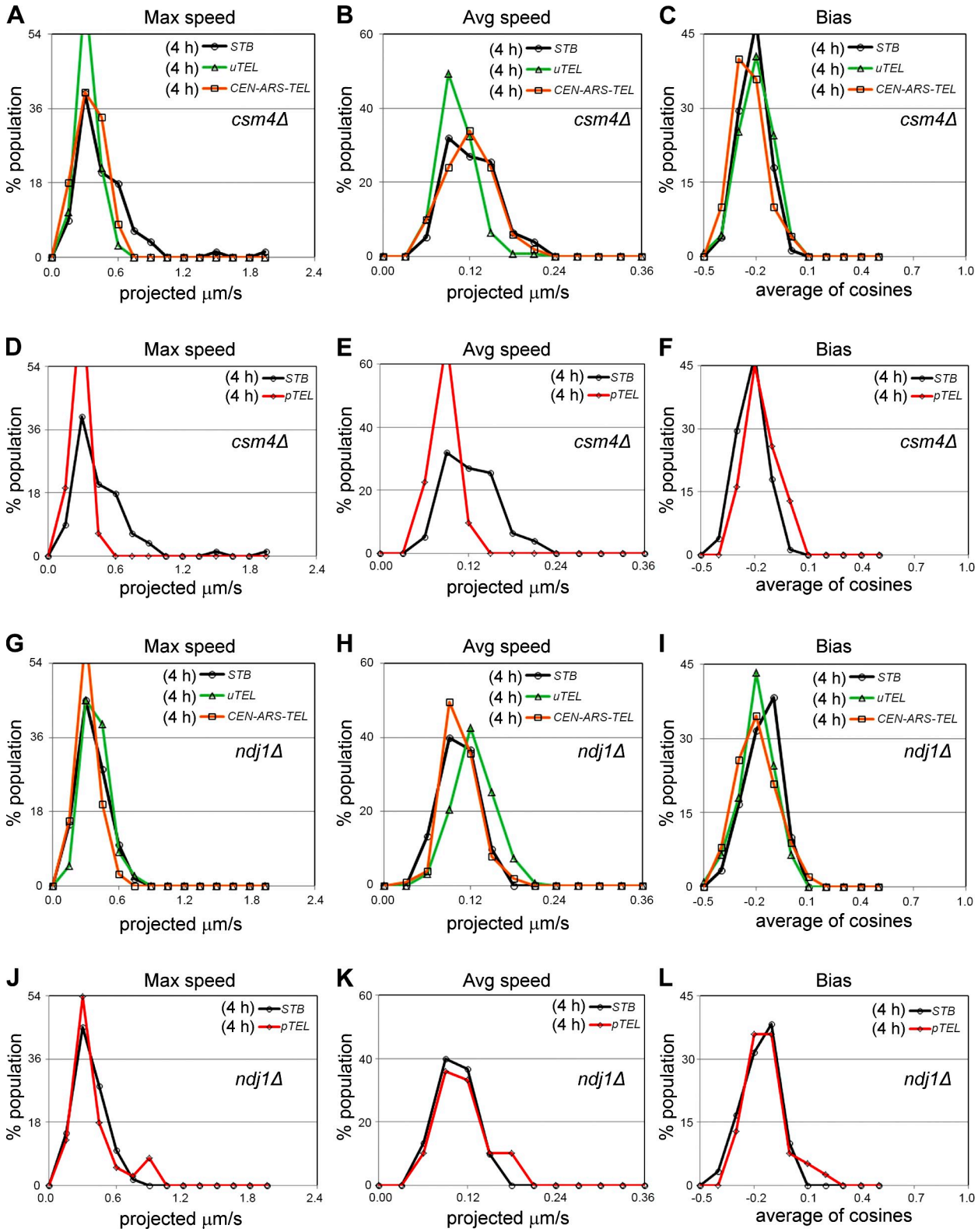

Figure S2. **Plasmid dynamics in *csm4Δ* and *ndj1Δ* strains at 4 h after transfer to sporulation medium.** The through-focus imaging results for the histogram representations shown here were obtained using the same procedures as in the experiments represented in Fig. 5 and Fig. 6. All the plots are based on data acquired at 1 frame/s. The results from the *csm4Δ* and *ndj1Δ* strains are arranged in A–F and G–L, respectively.

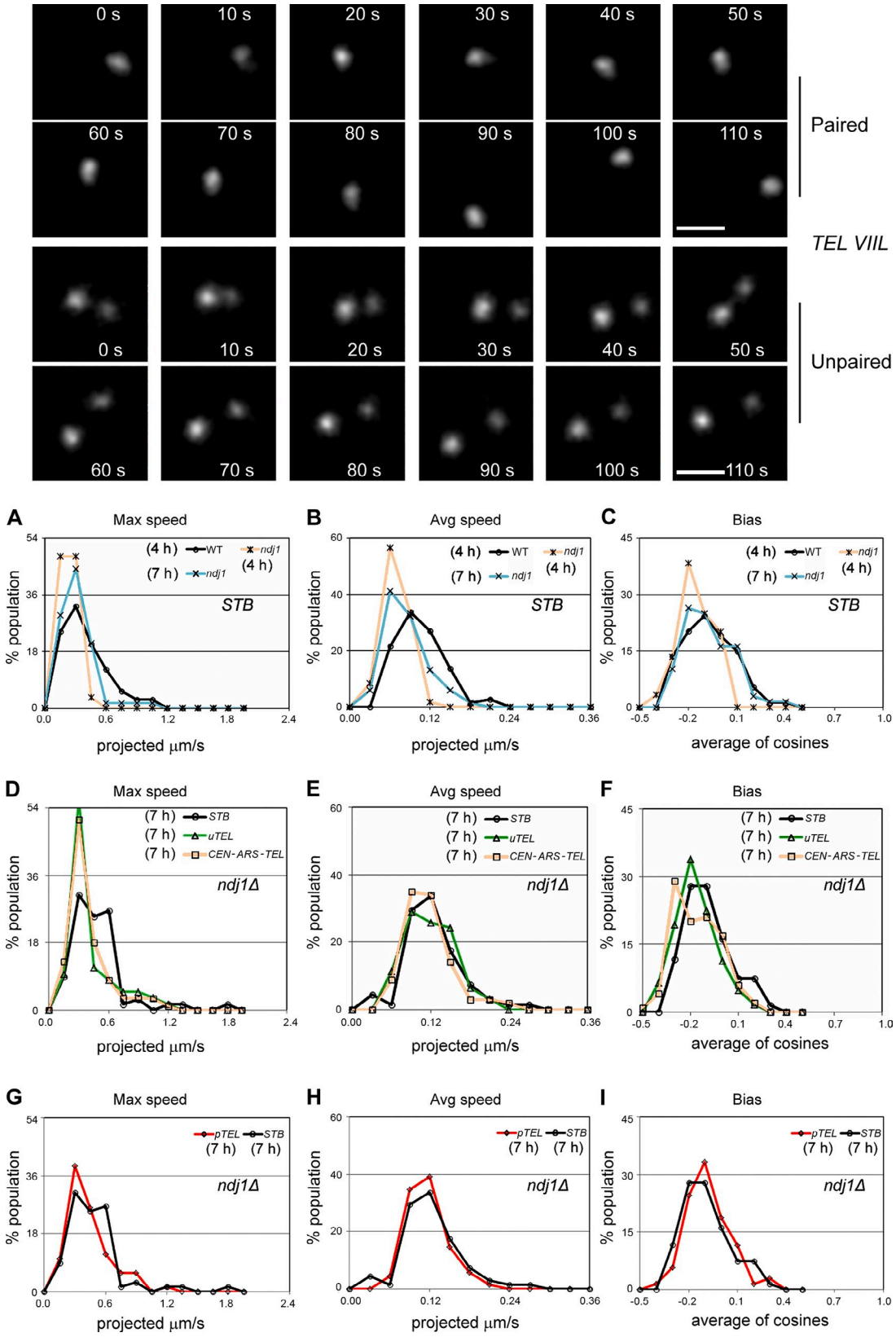

Figure S3. ***TEL* and *STB* plasmid dynamics in the wild-type and *ndj1Δ* strains.** An example of the time-lapse images of the fluorescence-tagged chromosome *VIIL TEL*s, followed as an internal reference during the analysis of the *STB* reporter plasmid in the wild-type strain (see Fig. 5), is shown at the top. Images containing a single spot and two separate spots represent paired and unpaired *TEL*s, respectively. The interval between the capture of each data frame was 2 s. Bars, 2 μm. In the panels below, plasmid and *TEL* dynamics, assayed in the *ndj1Δ* strain, are arranged as in Fig. 5. Comparisons of the *STB* reporter plasmid between wild-type (4 h) and the *ndj1Δ* (4 h and 7 h) strains (A–C) used data at 1 frame/2 s. As *ndj1Δ* slowed down meiosis, 4 h and 7 h in the wild-type and mutant strains, respectively, corresponded to the prophase stage. The dynamics of the *STB* plasmid were plotted against those of the *TEL* containing plasmid (D–F, *CEN-ARS-TEL*) or chromosome *IVR TEL*s (D–F, unpaired = u*TEL*; G–I, paired = p*TEL*). All of the comparisons within the mutant strain (D–I) were based on 1 frame/s data collected at 7 h for plasmids and for chromosomal *TEL*s. As explained in the legend for Fig. 6 and in the Materials and methods, the same dynamics data plotted with a time resolution of 1 frame/ 2 s (as in A–C) or 1 frame/s (as in D–I) will generate histograms of slightly different shapes. This difference is exemplified by the plots of the maximum speeds of the *STB* plasmid in the *ndj1Δ* mutant at 7 h in A versus D.

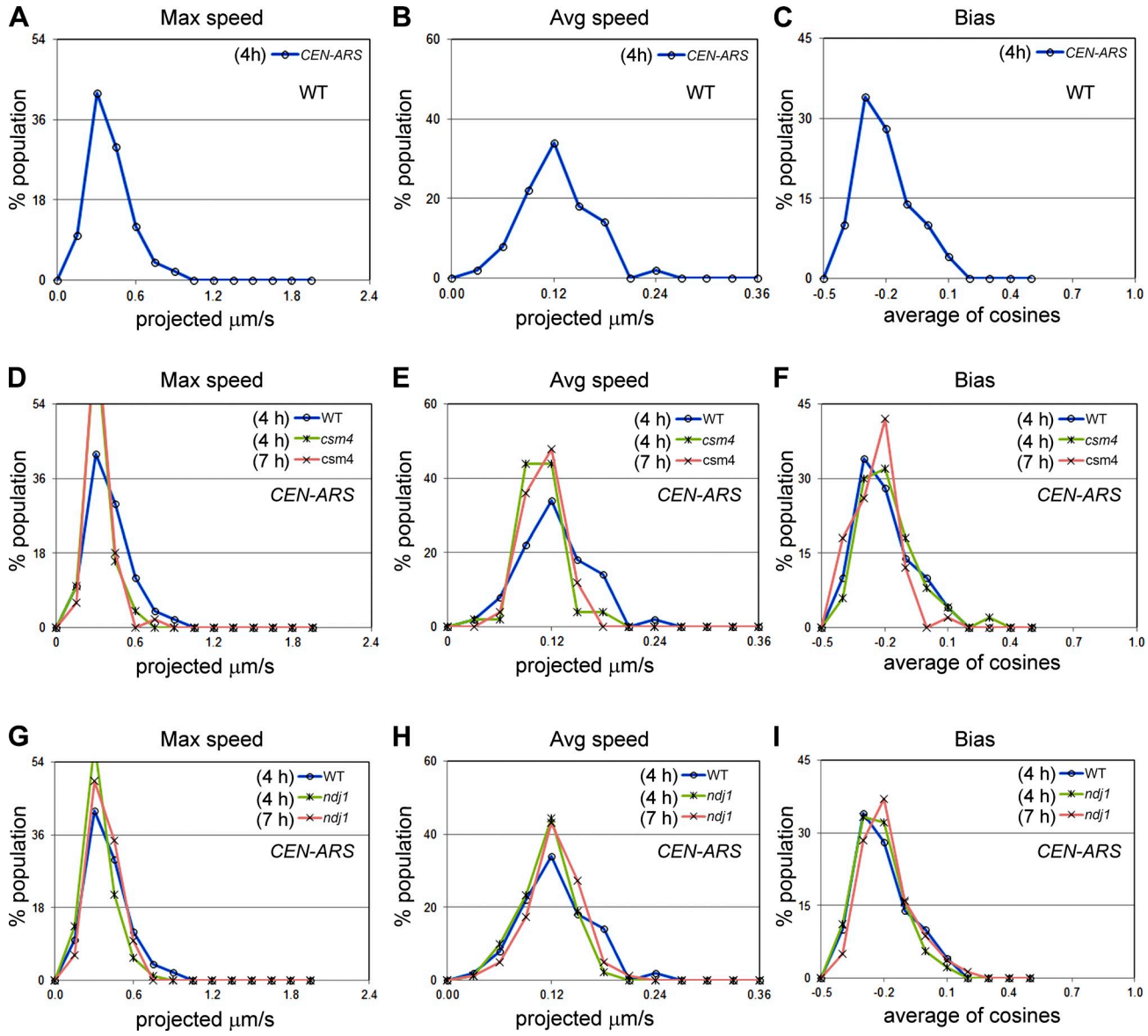

Figure S4. **Dynamics of a *CEN-ARS* plasmid in the wild-type, *ndj1Δ*, and *csm4Δ* strains.** The dynamics of a *CEN-ARS* plasmid in the wild-type strain (A–C) assayed at 4 h from the time of transfer to sporulation medium were placed in the context of its dynamics in the *csm4Δ* (D–F) and *ndj1Δ* strains (G–I) assayed at 4 h and 7 h after transfer to sporulation medium. These plots were based on data acquired at 1 frame/s.

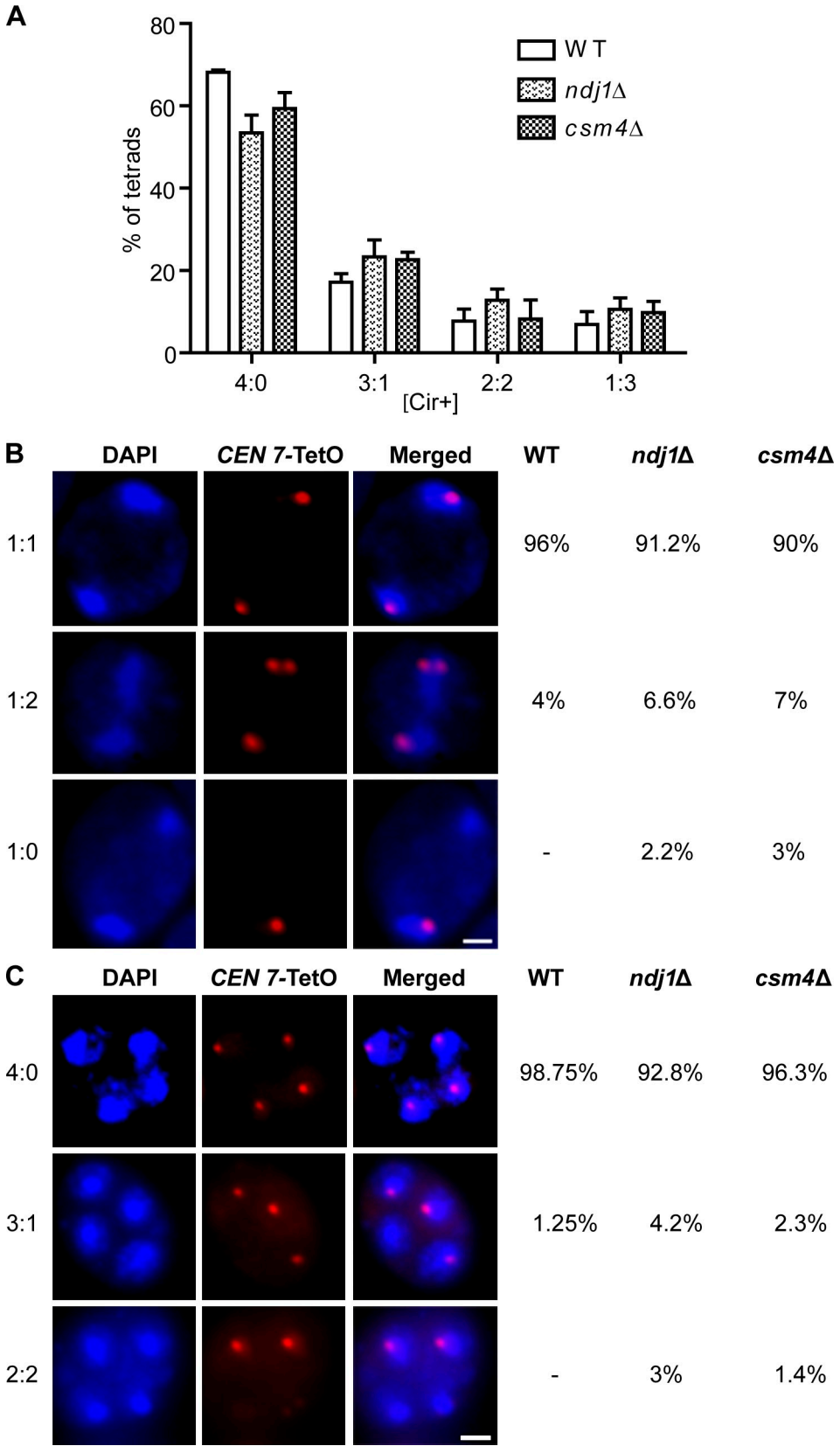

Figure S5. **Plasmid distribution in tetrads and meiotic chromosome segregation in the *ndj1Δ* and *csm4Δ* strains.** (A) The *STB* reporter plasmid segregation was assayed in the indicated [cir+] mutant strains at the end of meiosis II. The tetrads were classified by the plasmid distribution in the four spores as in Fig. S1. In the ratios below the x axis, the numbers at the left and the right denote plasmid-containing and plasmid-free spores, respectively. At least 100 tetrads were analyzed. The data for the wild type are taken from Fig. S1. (B and C) Chromosome *VII*, fluorescence-tagged at a *CEN*-proximal position in both homologues by [$TetO_{224}$-(TetR-td-Tomato)] interaction, served as the reporter. Segregation was assayed at the end of meiosis I (B) or at the end of meiosis II (C). The absence of a TetR fluorescent focus in one of the two nuclei in binucleate cells (B) indicated aberrant segregation of the homologues. In a small fraction of the normal segregation type, two fluorescent foci were observed in one nucleus, which suggests precocious sister chromatid separation. The presence of one or more spores (C) lacking a fluorescent focus in an ascus would be consistent with improper segregation during meiosis I or meiosis II or both. The error bars indicate ± SEM. Bars, 2 μm.

Table S1. **Strains**

Strain	Genotype	Relevant figures	Source/reference
MCY506 parent strain	MAT**a** *ade2 ADE5 CAN1^S cyh2^R his7-1 leu2::hisG lys2-2 met13-c trp1-63 tyr1-2 ura3-1* [cir+]	_	Conrad et al., 2007
MCY507 parent strain	MATα *ADE2 ade5 can1^R CYH2^S his7-2 leu2::hisG lys2-1 met13-d trp1-63 tyr1-1 ura3-13* [cir+]	_	Conrad et al., 2007
MJY8245	MJY8241 (*see below*) *tyr1::P_{URA3}-TetR-td-Tomato::TYR1 CEN VII::TetO224-TRP1* [cir+]	Figs. 1, 8, 10, S1, and S5	This study
MJY8248	MJY8242 (*see below*) *tyr1::P_{URA3}-TetR-td-Tomato::TYR1 CEN VII::TetO224-TRP1* [cir+]	Figs. 1, 8, 10, S1, and S5	This study
MJY8288	MCY506 *ura3::P_{HIS3}-GFP-LacI::URA3 lys2:: P_{DMC1}-GFP-LacI::LYS2* [cir0]	Fig. 2	This study
MJY8289	MCY507 *ura3::P_{HIS3}-GFP-LacI::URA3 lys2:: P_{DMC1}-GFP-LacI::LYS2* [cir0]	Fig. 2	This study
MJY8319	MJY8241 (*see below*) *MPS3-3HA::TRP1 CTF19-13Myc::KANMX6* [cir+]	Figs. 2 and 3	This study
MJY8320	MJY8242 (*see below*) *MPS3-3HA::TRP1 CTF19-13Myc::KANMX6* [cir+]	Figs. 2 and 3	This study
EAY1542	MATα *ho::hisG his4X-LEU2-URA3 leu2::hisG RAP1-mRFP-HPHMX ura3(ΔSmaI-PstI)* [cir+]	–	Wanat et al., 2008
MJY8359	MAT**a** *ade2 trp1-63 leu2::hisG his7-1/2 ura3::P_{HIS3}-GFP-LacI::URA3 lys2:: P_{DMC1}-GFP-LacI::LYS2 RAP1-mRFP-HPHMX* [cir+]	Fig. 3	This study EAY1542 X MJY8241
MJY8362	MATα *ade2 trp1-63 leu2::hisG his7-1/2 ura3::P_{HIS3}-GFP-LacI::URA3 lys2:: P_{DMC1}-GFP-LacI::LYS2 RAP1-mRFP-HPHMX* [cir+]	Fig. 3	This study EAY1542 X MJY8241
MJY8279	MCY506 *ZIP1::GFP^{700}* [cir+]	Fig. 4	This study
MJY8280	MCY507 *ZIP1::GFP^{700}* [cir+]	Fig. 4	This study
MJY8241	MCY506 *ura3::P_{HIS3}-GFP-LacI::URA3 lys2:: P_{DMC1}-GFP-LacI::LYS2* [cir+]	Fig. 4	This study
MJY8242	MCY507 *ura3::P_{HIS3}-GFP-LacI::URA3 lys2:: P_{DMC1}-GFP-LacI::LYS2* [cir+]	Fig. 4	This study
MDY1567	MCY506 *TUB1-GFP-URA3 LYS2::P_{DMC1}-LacI/GFP URA3::CYC1::P_{CYC1}-lacI-GFP TELIVR::*LacO256-*LEU2* [cir+]	Fig. 5	Conrad et al., 2008
MDY2426	MCY507 *URA3::P_{DMC1}-LacI/GFP CYC1::P_{CYC1}-lacI-GFP TELIVR::*LacO256-*LEU2* [cir+]	Fig. 5	Conrad et al., 2008
MDY2414	MCY506 *ura3::P_{HIS3}-GFP-LacI::URA3 CYC1:: P_{CYC1}-GFP-LacI* [cir+]	Figs. 5 and S4	This study
MDY2798	MCY507 *lys2:: P_{DMC1}-GFP-LacI::LYS2* [cir+]	Figs. 5 and S4	This study
MJY8247	MJY8241 *tyr1::P_{URA3}-TetR-td-Tomato::TYR1 TEL VIIL::*TetO224-*TRP1* [cir+]	Figs. 5, 6, and S3	This study
MJY8250	MJY8242 *tyr1::P_{URA3}-TetR-td-Tomato::TYR1 TEL VIIL::*TetO224-*TRP1* [cir+]	Figs. 5, 6, and S3	This study
MDY2778	MCY506 *TUB1-GFP-URA3 LYS2::P_{DMC1}-LacI/GFP URA3::CYC1::P_{CYC1}-lacI-GFP TELIVR::*LacO256-*LEU2 csm4Δ::LEU2* [cir+]	Figs. 6 and S2	Conrad et al., 2008
MDY2609	MCY507 *URA3::P_{DMC1}-LacI/GFP CYC1::P_{CYC1}-lacI-GFP TELIVR::*LacO256-*LEU2 csm4Δ::LEU2* [cir+]	Figs. 6 and S2	Conrad et al., 2008
MCY2515	MCY506 *TUB1-GFP-URA3 lys2:: P_{DMC1}-GFP-LacI::LYS2 csm4Δ::TRP1* [cir+]	Figs. 6 and S2	This study
MCY2514	MCY507 *ura3::P_{HIS3}-GFP-LacI::URA3 CYC1:: P_{CYC1}-GFP-LacI csm4Δ::TRP1* [cir+]	Figs. 6 and S2	This study
MCY1850	MCY506 *ura3::P_{HIS3}-GFP-LacI::URA3 CYC1:: P_{CYC1}-GFP-LacI csm4Δ::TRP1* [cir+]	Figs. 6, S2 and S4	This study
MCY1851	MCY507 *lys2:: P_{DMC1}-GFP-LacI::LYS2 csm4Δ::TRP1*[cir+]	Figs. 6, S2, and S4	This study
MJY8391	MJY8248 + YCp-*URA3-Nup49-mCherry-HIS7* (pSS50) [cir+]	Fig. 8	This study
MJY8392	MJY8344 (*see below*) + YCp-*URA3-Nup49-mCherry-HIS7* (pSS50) [cir+]	Fig. 8	This study
MJY8393	MJY8347 (*see below*) + *YCp-URA3-Nup49-mCherry-HIS7* (pSS50) [cir+]	Fig. 8	This study
MJY8375	MJY8359 *ndj1Δ::KANMX6* [cir+]	Fig. 9	This study
MJY8377	MJY8362 *ndj1Δ::KANMX6* [cir+]	Fig. 9	This study
MJY8343	MJY8245 *ndj1Δ::KANMX6* [cir+]	Figs. 8, 10, and S5	This study
MJY8344	MJY8248 *ndj1Δ::KANMX6* [cir+]	Figs. 8, 10, and S5	This study
MJY8346	MJY8245 *csm4Δ::KANMX6* [cir+]	Figs. 8, 10, and S5	This study
MJY8347	MJY8248 *csm4Δ::KANMX6* [cir+]	8, 10 and S5	This study
MDY1560	MCY506 *TUB1-GFP-URA3 LYS2::P_{DMC1}-LacI/GFP URA3::CYC1::P_{CYC1}-lacI-GFP TELIVR::*LacO256-*LEU2 ndj1Δ::TRP1* [cir+]	Figs. S2 and S3	Conrad et al., 2008
MDY2294	MCY507 *URA3::P_{DMC1}-LacI/GFP CYC1::P_{CYC1}-lacI-GFP TELIVR::*LacO256-*LEU2 ndj1Δ::TRP1* [cir+]	Figs. S2 and S3	Conrad et al., 2008
MCY3161	MCY506 *lys2:: P_{DMC1}-GFP-LacI::LYS2 ndj1Δ::TRP1* [cir+]	Figs. S2, S3, and S4	This study
MDY2344	MCY507 *ura3::P_{HIS3}-GFP-LacI::URA3 CYC1:: P_{CYC1}-GFP-LacI ndj1Δ::TRP1* [cir+]	Figs. S2, S3, and S4	This study

The yeast strains utilized for the present study are listed. The relevant genotypes are indicated. The diploid strains for plasmid segregation, localization, and dynamics assays were constructed anew for each set of assays. The reporter plasmid was introduced into the desired "a" mating type strain by transformation, and the transformant was mated with the "α" mating type partner strain. Strains carrying or lacking endogenous 2 micron plasmid are designated as [cir+] or [cir0], respectively. The list is arranged roughly to conform to the sequence in which the results are presented. An experiment in which a particular strain or a plasmid was utilized is denoted by qualifying it with the appropriate figure number. The relevant references are cited.

Table S2. **Plasmids**

Plasmids	Salient features	Relevant figures	Source/reference
YEp181LacO	$LacO_{256}$ cloned in YEp181 (*LEU2*)	Figs. 1–6, 8–10, S1–S3, and S5	Mehta et al., 2002
pSLB5	$LacO_{256}$ cloned in *ARS1-LEU2* vector	Figs. 1 and S1	Lacefield et al., 2009
pSV31	P_{HIS3}-*GFP-LacI* cloned in YIp-*URA3* (pRS406)	Figs. 1–6, 8–10, and S1–S5	M.J. laboratory
pSS18	*TYR1* cloned in P_{URA3}-*TetR-td-Tomato-LEU2* plasmid	Figs. 1, 5, 6, 8, 10, S1, S3, and S5	This study
pSS22	P_{DMC1}-*GFP-LacI* cloned in YIp-*LYS2*	Figs. 1–6, 8–10, and S1–S5	This study
pSS35	$TetO_{224}$ target at 479,261 bp (*CEN VII*)	Figs. 1, 8, 10, S1, and S5	This study
pSS38	$TetO_{224}$ target at 4,161 bp (*VIIL TEL*)	Figs. 5, 6, and S3	This study
LF321 (pHW122)	GFP inserted at 700 amino acid of *ZIP1* ORF resulted ZIP1::GFP^{700}	Fig. 4	Scherthan et al., 2007
MCB831	$LacO_{256}$ cloned in *CEN-ARS* vector (YCp111)	Figs. 5 and S4	This study
MCB832	Yeast *TEL* repeat cloned in MCB831	Figs. 5, 6, S2, and S3	This study
pAJ2979	Nup49-mCherry cloned in YCp-*URA3*	–	Gift from Arlen Johnson
pSS50	*HIS7* cloned in pAJ2979	Fig. 8	This study

The plasmids utilized for the present study are listed, and their relevant features are indicated. The list roughly follows the sequence in which the results are presented. The figure numbers refer to the figure representing the experiments in which a particular plasmid was utilized. The relevant references are cited.

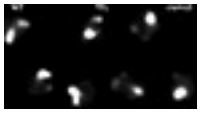

Video 1. **Chromosome dynamics in wild-type and *csm4Δ* cells.** In this time-lapse video analysis, chromosome *IVR* telomere was labeled [$LacO_{256}$-(LacI-GFP)] in both homologues. Through-focus images were acquired at 1 frame/s in wild-type cells at 4 h after transfer to sporulation medium (left). Similar analysis was performed in *csm4Δ* cells at 8 h after transfer to sporulation medium (right). The data from this video are displayed in Fig. 5 (A–F) and Fig. 6 (D–I). The large bright spot (seen also in the *csm4Δ* panel of Video 2 and in Video 3) is the spindle pole body labeled with Tub1-GFP. WT, wild type; *TEL*, chromosome *IVR* telomere. Images were taken at 27°C, with 250-ms exposures with a pixel spacing of 0.0645 µm using an upright microscope (Axioplan 2ie) fitted with a 100×, 1.4 NA Plan-Apochromat objective lens (Carl Zeiss), a high-speed switching DG-5 xenon illuminator (Sutter Instrument), a CoolSNAP HQ digital camera (Photometrics), and a BNC555 pulse generator (Berkeley Nucleonics) to synchronize camera exposure with focusing movements and illumination. Image acquisition, deconvolution, viewing, and quantification were carried out using custom-written software.

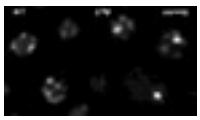

Video 2. **Plasmid dynamics in wild-type and *csm4Δ* cells.** Time-lapse video analysis of the fluorescence tagged *STB* reporter plasmid [$LacO_{256}$-(LacI-GFP)] was performed at 4 h (in the wild-type strain; left) and 7 h (in the *csm4Δ* strain; right) after cells were transferred to sporulation medium. Images were acquired at 1 frame /2 s in wild type and at 1 frame/s in *csm4Δ* cells. The data derived from these videos are shown in Fig. 5 (A–I), Fig. 6 (A–I), and Fig. S3 (A–C). WT, wild type. Images were taken at 27°C, with 250-ms exposures with a pixel spacing of 0.0645 µm using an upright microscope (Axioplan 2ie) fitted with a 100×, 1.4 NA Plan-Apochromat objective lens (Carl Zeiss), a high-speed switching DG-5 xenon illuminator (Sutter Instrument), a CoolSNAP HQ digital camera (Photometrics), and a BNC555 pulse generator (Berkeley Nucleonics) to synchronize camera exposure with focusing movements and illumination. Image acquisition, deconvolution, viewing, and quantification were carried out using custom-written software.

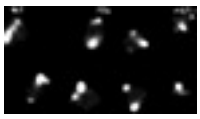

Video 3. **Chromosome dynamics in wild-type and *ndj1Δ* cells.** The chromosome and spindle pole bodies were labeled as described for Video 1. Images were acquired at 1 frame/s at 4 h (wild type) and 7 h (*ndj1Δ*) after transferring cells to sporulation medium. The wild-type cells shown here are the same as those in Video 1. The data corresponding to the *ndj1Δ* panel are displayed in Fig. S3 (D–I). WT, wild type; *TEL*, chromosome *IVR* telomere. Images were taken at 27°C, with 250-ms exposures with a pixel spacing of 0.0645 µm using an upright microscope (Axioplan 2ie) fitted with a 100×, 1.4 NA Plan-Apochromat objective lens (Carl Zeiss), a high-speed switching DG-5 xenon illuminator (Sutter Instrument), a CoolSNAP HQ digital camera (Photometrics), and a BNC555 pulse generator (Berkeley Nucleonics) to synchronize camera exposure with focusing movements and illumination. Image acquisition, deconvolution, viewing, and quantification were carried out using custom-written software.

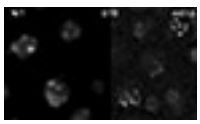

Video 4. ***STB* plasmid dynamics in wild-type and *ndj1Δ* cells.** Time-lapse images of the *STB* plasmid foci [$LacO_{256}$-(LacI-GFP)] were acquired at 1 frame/ 2 s in wild-type cells and at 1 frame/s in *ndj1Δ* cells. The analyses were done at 4 h (wild type) and 7 h (*ndj1Δ*) after transferring cells to the sporulation medium. The wild-type cells shown here and in Video 2 are identical. The data derived from the *ndj1Δ* video are shown in Fig. S3 (A–I). WT, wild type. Images were taken at 27°C, with 250-ms exposures with a pixel spacing of 0.0645 µm using an upright microscope (Axioplan 2ie) fitted with a 100×, 1.4 NA Plan-Apochromat objective lens (Carl Zeiss), a high-speed switching DG-5 xenon illuminator (Sutter Instrument), a CoolSNAP HQ digital camera (Photometrics), and a BNC555 pulse generator (Berkeley Nucleonics) to synchronize camera exposure with focusing movements and illumination. Image acquisition, deconvolution, viewing, and quantification were carried out using custom-written software.